

Portland State University PDXScholar

Civil and Environmental Engineering Faculty
Publications and Presentations

Civil and Environmental Engineering

2008

Suspended Sediment Fluxes at an Intertidal Flat: The Shifting Influence of Wave, Wind, Tidal, and Freshwater Forcing

Stefan A. Talke


Portland State University, talke@pdx.edu

Mark T. Stacey

University of California at Berkeley

Let us know how access to this document benefits you.

Follow this and additional works at: https://pdxscholar.library.pdx.edu/cengin_fac

 Part of the [Civil Engineering Commons](#), and the [Environmental Engineering Commons](#)

Citation Details

Talke, Stefan A. and Stacey, Mark T., "Suspended Sediment Fluxes at an Intertidal Flat: The Shifting Influence of Wave, Wind, Tidal, and Freshwater Forcing" (2008). *Civil and Environmental Engineering Faculty Publications and Presentations*. 84.
https://pdxscholar.library.pdx.edu/cengin_fac/84

This Post-Print is brought to you for free and open access. It has been accepted for inclusion in Civil and Environmental Engineering Faculty Publications and Presentations by an authorized administrator of PDXScholar. For more information, please contact pdxscholar@pdx.edu.

Suspended sediment fluxes at an intertidal flat: The shifting influence of wave, wind, tidal, and freshwater forcing

Stefan A. Talke¹, Mark T. Stacey²

(1): Institute for Marine and Atmospheric research, University of Utrecht,
Princetonplein 5, 3584 CC Utrecht, the Netherlands,
e-mail: s.a.talke@phys.uu.nl

(2): Department of Civil and Environmental Engineering, University of California at Berkeley,
Berkeley, CA, 94720 USA
e-mail: m.stacey@berkeley.edu

Keywords: Intertidal Mudflat, Sediment Transport, Waves, Tides, Seiching, USA, California, San Francisco Bay

Abstract

Using in-situ, continuous, high frequency (8 – 16 Hz) measurements of velocity, suspended sediment concentration (SSC), and salinity, we investigate the factors affecting near-bed sediment flux during and after a meteorological event (cold front) on an intertidal flat in central San Francisco Bay. Hydrodynamic forcing occurs over many frequency bands including wind-wave, ocean swell, seiching (500-1000 second), tidal, and infra-tidal frequencies, and varies greatly over the time scale of hours and days. Sediment fluxes occur primarily due to variations in flow and SSC at three different scales: residual (tidally averaged), tidal, and seiching. During the meteorological event, sediment fluxes are dominated by increases in tidally-averaged SSC and flow. Runoff and wind-induced circulation contribute to an order of magnitude increase in tidally averaged offshore flow, while waves and seiching motions from wind forcing cause an order of magnitude increase in tidally averaged SSC. Sediment fluxes during calm periods are dominated by asymmetries in SSC over a tidal cycle. Freshwater forcing produces sharp salinity fronts which trap sediment and sweep by the sensors over short (~ 30 minute) time scales, and occur primarily during the flood. The resulting flood dominance in SSC is magnified or reversed by variations in wind-forcing between the flood and ebb. Long term records show that more than half of wind events (sustained speeds of greater than 5 m/s) occur for three hours or less, suggesting that asymmetric wind forcing over a tidal cycle commonly occurs. Seiching associated with wind and its variation produces onshore sediment transport. Overall, the changing hydrodynamic and meteorological forcing influence sediment flux at both short (minutes) and long (days) time scales.

1. Introduction

Intertidal flats form a boundary between land and sea, and are important feeding grounds for birds, fish, and other biota. Moreover, due to their proximity to cities and industrial areas, intertidal flats may contain buried contaminants that are uncovered by storm events and long-term morphological change. Thus, the physical processes that create, erode and rework intertidal flats are immensely important from both an ecological and practical viewpoint.

Previous studies have suggested that the primary forces shaping intertidal flats are wind-induced waves and tidal currents. The shifting influence of wind has generally been reduced

50 to three distinct levels of forcing conditions: stormy, windy, and calm (Shi and Chen, 1996,
51 Le Hir et al, 2000, Janssen- Stelder, 2000). During storms, large waves are observed to erode
52 sediment and keep sediment in suspension during the slack tide, which is then available to be
53 transported offshore during the ebb (Le Hir et al, 2000, Dyer et al, 2000, Bassoullet et al,
54 2000, Andersen & Perjup, 2001). Storms may also deposit sediments onto upland marshes
55 (e.g., Yang et al, 2003, and list therein). During windy periods, local erosion generally
56 results in offshore transport (Christie et al., 1999), Dyer et al., 2000, de Jonge and van
57 Beusekom, 1995), though net transport can be onshore as well (e.g., de Haas and Eisma,
58 1993). During calm periods, net transport is observed to be onshore (Black, 1998, Christie et
59 al., 1999, Dyer et al, 2000, Le Hir et al., 2000, Ridderinkhof et al, 2000), which is attributed
60 to settling lag and scour lag effects (Christie et al, 1999). Sediment is observed to be eroded
61 during the flood tide, is transported shoreward, and settles out during the high-water slack
62 period (Christie et al, 1999; de Haas & Eisma, 1993; Ridderinkhof et al. 2000). Because ebb
63 currents are insufficient to resuspend and transport all the recently deposited sediment (even
64 in an ebb dominated estuary such as the Dollard, NL), accretion occurs in calm periods (Dyer
65 et al, 2000).

66
67 Models of sediment transport have provided important insights into intertidal processes by
68 focusing on the effects of tidal currents (Friedrichs & Aubrey, 1996, Pritchard et al., 2002,
69 Pritchard & Hogg., 2003), or the combined affect of winds and tidal currents (Ridderinkhof,
70 1998, Roberts et al., 2000, Waeles et al., 2004). Sediment fluxes are found to occur due to
71 tidal asymmetries in velocity (e.g., Ridderinkhof, 1998, Roberts et al., 2000, Pritchard et al.,
72 2002) and due to settling lag effects (e.g., Pritchard & Hogg, 2003). Ridderinkhof (1998)
73 concludes that asymmetries in tidal velocities (rather than waves) set the direction of sediment
74 flux, and that waves reduce net sediment flux by keeping sediment in suspension over a tidal
75 cycle. Waeles et al. (2004) finds that even small (but constantly applied) waves of 5 cm cause
76 an export of sediment that is balanced by input at the seaward boundary. All models that
77 include wave effects apply constant forcing over a tidal period (e.g., Ridderinkhof, 1998,
78 Roberts et al., 2000, Waeles et al., 2004).

79
80 Other factors besides wind waves and tidal currents are observed to play a role in sediment
81 erosion and transport over a tidal time scale. Ridderinkhof et al. (2000) and de Haas and
82 Eisma (1993) note that storm surge increases SSC and offshore transport in the Ems/Dollard
83 estuary. Storm surge also increases the influx of sediments to upland marshes, particularly
84 during spring tides (Yang et al, 2003). Christiansen et al. (2006) found that asymmetries in
85 tidal velocity caused by winds of 4-12 m/s dominated sediment fluxes at a tidal flat in the
86 Wadden Sea. Freshwater flow from upland watersheds or local rain runoff affects the mean
87 current, as can local circulation patterns, nonlinear waves (Stokes drift), wind stress, and
88 many other sources (Le Hir et al., 2000). Changes to the supply of sediment (Ridderinkhof et
89 al 2000, Wright and Schoellhamer, 2004) or the critical stress of erosion (Kornman and de
90 Deckere, 1998, Staats et al, 2001, O'Brien et al., 2000, Dyer, 1998) are important components
91 of the long-term sediment balance. All these factors show that erosion, deposition, and
92 transport are subject to many changeable parameters.

93
94 In this contribution we explore the subtle effects of changes in hydrodynamic and
95 meteorological forcing from short time scales (wave time scale) to longer time scales (days)
96 on an intertidal flat in San Francisco Bay. We investigate the mechanisms that elevate SSC,
97 including waves, tidal currents, seiche motions, and freshwater forcing, and evaluate the
98 time scales over which SSC and velocity vary. In turn we highlight how variations at both
99 tidally-averaged and intra-tidal time scales affect net sediment fluxes during a meteorological

100 event (cold front) and a relatively calmer period. We show that the relative phasing (timing)
101 and time-scales of wind, tidal and freshwater forcing can completely alter the net flux of
102 sediment in the intertidal zone, even between consecutive tidal periods.

103

104 In Section 2 we describe the experiment site and measurement methods, while in section 3 we
105 describe the hydrographic results and explore the variations of SSC and sediment flux. In
106 section 4 we analyze sediment flux at the tidally averaged and tidally varying time scales, and
107 the conclusions are presented in section 5.

108

109

110 2. Methods

111

112 The intertidal flat we investigate in this study is situated in the central San Francisco Bay near
113 the city of Richmond, CA (figure 1a). Along its east and west borders, the intertidal flat is
114 fringed by marshland (figure 1b) that lies behind an outer seawall. The northern border is a
115 rip-rap seawall. Two subtidal channels drain the upland marsh system and combine together
116 within the intertidal flat. The southern side of the intertidal flat, roughly 200 m in diameter, is
117 open to the central San Francisco Bay. The sediment is dominated by fine sand and silt, and
118 shape of the mudflat morphology is convex upwards, consistent with an accretionary flat
119 (Dyer, 1998, Le Hir et al, 2000, Kirby, 2000). Ripples with a wavelength of 0.05-0.06 m and
120 a height of 0.01-0.02 m occur on the flat.

121

122 Over a four day period beginning at 16:00 hrs (local time) on April 11, 2003 and ending at
123 17:00 hrs on April 15th, 2003 we deployed an array of hydrodynamic sensors on a sawhorse
124 frame (figure 2) located at the opening of the flat to the bay (see figure 1). The frame was
125 located about 50 m west of the subtidal channel, and oriented along the primary (North-
126 South) stream axis. The frame is thus optimally oriented to observe fluxes between the
127 central bay and the flat. On the frame we deployed 6 Acoustic Doppler Velocimeters
128 (ADV), 3 optical backscatter sensors (OBS) from D&A instruments, 3 Conductivity-
129 Temperature-Depth sensors (CTDs), and 2 combined OBS/Fluorometers. The OBS was
130 calibrated by Ralston (2005) using estimates of SSC found from co-located, in-situ water
131 samples.

132

133 The velocimeters and turbidity sensors were located at heights between 0.01 m and 0.35 m off
134 the bed, and measured a new, synchronous 'burst' of data every 10 minutes. Nearly
135 continuous velocity data (burst length of 590 seconds) was measured at heights of 0.16 m and
136 0.28 m at a frequency of 8 Hz, and was synchronized with OBS sensors at 0.05 m and 0.19 m.
137 The accuracy of the velocimeters is estimated by the manufacturers to be 0.001 m/s. Because
138 of memory and battery constraints, the remaining velocimeters measured for burst lengths of
139 either 188 seconds (side-mounted) or 345 seconds. A small portion (order of 10-20 minutes)
140 of each flood and ebb period was missed until the sensors were immersed. Additionally, the
141 side-mounted velocimeters (0.1 m and 0.33 m off bed), the two lower downward facing
142 velocimeters (0.01 m and 0.05 m off bed), and the lower OBS (0.05 m off bed) failed during
143 the large cold front that occurred from April 11th-April 13th, 2003. Finally, during the cold
144 front, changes to the relative bed-level of 0.05 m to 0.1 m (the frame settled into the sediment)
145 biased velocity and SSC measurements. The frame was repositioned relative to the bed after
146 tide 4 to the initial specifications. Because of the data limitations, we focus on mechanisms of
147 near-bed suspended sediment transport for the velocity/SSC pair deployed at 0.16 m and 0.19
148 m, realizing that the height off the bed was $O(0.1 \text{ m})$ during portions of the meteorological
149 event.

150
151 We obtained hourly wind speed data from a meteorological station located ~ 1 km from the
152 experiment site (Bay Area Air Quality Management District station 2950). Water level data
153 was obtained from NOAA buoy 9414863 at the Chevron Oil Pier in Richmond. The publicly
154 available tidal prediction software Jtides was used to compare predicted tidal levels to the
155 actually measured tidal levels.

156
157

158 **3. Results**

159

160 Below we describe the hydrodynamic conditions prevalent during the experiment, and the
161 sediment fluxes resulting from them. Because hydrodynamic conditions varied during the
162 meteorological event (hour 0-50) and afterwards (hour 50-100), we summarize the
163 hydrographic conditions in Fig. 3 and Fig. 4, respectively.

164

165 **3.1 Hydrographic conditions**

166

167 The central San Francisco Bay is forced by semi-diurnally varying tides with a maximum
168 tidal range of ~ 2 m. During the first four tidal periods (Fig. 3a) of the experiment, the diurnal
169 inequality is evident in the water-level amplitude (1.1 m -1.5 m), while by contrast the second
170 four tides are nearly equal in amplitude (~1.5 m; Fig. 4a). The cross-shore, north-south tidal
171 current V_{30} , as measured by a 30 minute moving average, typically exhibits a maximum of
172 0.07 m/s – 0.11 m/s with-in an hour of wetting or drying (see Fig. 3b and 4b), with the
173 exception of an ebb flow of 0.25 m/s during the late ebb at $t=20-21$ hours (Fig. 3b).

174

175 Between April 11th and April 13th, 2003, a large cold front passed through the San Francisco
176 Bay area. The peak of the meteorological event occurred between $t=11$ hours and $t=19$ hours
177 from the start of the experiment (i.e., during tide 2), with sustained winds of greater than 9
178 m/s (see Fig. 3c). Wind velocity reduced to a range of 4.5 m/s – 7 m/s between hour 20 to
179 hour 35, and to 4-6 m/s between hour 40 and hour 50. After the meteorological event, periods
180 of moderate wind (3-5 m/s) occur between hour 50-52, hour 70-80, and hour 90-100.

181 Between $t=53$ hours and $t=88$ hours, wind was directed offshore (from north to south), as
182 indicated by the dotted line.

183

184 A comparison of measured and predicted water levels show that winds caused a surge of ~
185 0.25 m by $t=20$ hours, and reached a maximum of ~ 0.3 m at $t=30$ hours. Elevated water
186 levels persisted through tide 4 (0.2 m at High Water) and tide 5 (0.06 m at High Water) but
187 became insignificant for tides 6-8. The surge coincided with seiching motions with velocities
188 of 0-0.15 m/s and a period of ~ 500-1000 seconds. These seiching motions occur primarily
189 during tides 2-5, and are shown by the envelope created by the 1-minute mean velocity (Fig.
190 3b and Fig. 4b). As wind-setup disappears during tides 6-8, seiching motions become small.

191

192 Precipitation from the meteorological event increased the freshwater discharge in the subtidal
193 creek, and began lowering salinity concentrations starting at ~ $t=17$ hours. During the
194 meteorological event, large variation between bay water (> 20 psu) and fresher water (< 10
195 psu) were observed during wetting and drying. The effect of freshwater discharge was also
196 observed at high water (HW), as salinity decreased from 25.8 psu during tide 1 to a minimum
197 of 23.2 psu during tide 3 (Fig. 3d). After the meteorological event, the salinity at high water
198 slowly increases, from 24.3 psu at $t=55$ hours to 26.1 psu at $t=92$ hours (figure 4d).

199 Similarly, the differences in salinity over a tidal period lessen.

200
201 As shown in Fig. 3e and Fig. 4e, the characteristic profile of suspended sediment
202 concentration (SSC) over an immersed period includes a period of elevated sediment
203 concentration during the flood, a reduction during the slack period, and a corresponding
204 increase during the ebb (see figure 4e). Overall, the tidally averaged concentration increases
205 from 0.11 kg/m^3 during tide 1 to a peak of 0.19 kg/m^3 during tide 4, then reduces to 0.02
206 kg/m^3 by tide 7 (post-event). The source of variation in SSC over the experiment is the focus
207 of the next section.

208
209 The evolution of wave orbital velocity and energy over the experiment is depicted in Fig. 3c,
210 Fig. 4c., and Fig. 5. The rms wave orbital velocity (estimated using an averaging time of 20
211 minutes after removing the 1 minute mean velocity), decreases from a maximum of 0.24 m/s
212 during the meteorological event to a maximum of 0.12 m/s in tides 5-8 (compare Fig. 3c and
213 4c). Near-bed wave energy was typically smallest at high tide since orbital motions decay
214 more with depth during periods of high water (for the same wave conditions).

215
216 Fig. 5 compares the power spectrum of velocity during the flood and ebb period of each tidal
217 period. Three bands of energy are evident: locally forced wind waves between 0.25 Hz and 1
218 Hz, offshore ocean swell between 0.05 and 0.15 Hz, and intra-tidal motions between $3 \cdot 10^{-3}$
219 Hz and $8 \cdot 10^{-4}$ Hz. Wind induced wave energy is largest during tide 2, and decreases in
220 spectral energy and average period ($T=1/f$) occur as wind-forcing decreases in succeeding
221 tides (see also Fig. 3c). After the flood of tide 5, no appreciable wind-wave energy is evident
222 until the ebb of tide 8. However, waves at the ocean swell frequency persist after local wind
223 forcing vanishes (see also Talke & Stacey, 2003), and are the largest component of wave
224 forcing from the ebb of tide 5 through the flood of tide 7. At lower frequencies, two peaks of
225 energy are persistently found at periods of 500 seconds ($2 \cdot 10^{-3}$ Hz) and at 900-1000 seconds.
226 These intra-tidal motions, which we collectively call 'seiching', are largest during the windy
227 periods from tide 1 through tide 5. Differences in energy between flood and ebb are
228 characteristic for all energy bands, and are particularly well defined for tides 4, 5, and 8
229 (wind-waves), tide 5 and tide 7 (ocean swell) and tide 4, 7 and 8 (intra-tidal motions).

230 231 **3.2 Analysis of SSC on flat**

232
233 In this section we investigate whether wind causes the variation in waves and SSC at the
234 experiment site by developing a regression between wind, wind-waves, and SSC (Fig. 6).
235 Fig. 6c shows the least-squares fit to a scatter plot of the 1 hour mean wind energy and the 1
236 hour mean wind-wave energy. Because the fit of the line is good ($R^2 = 0.78$), our
237 measurements indicate that on average, wave energy is linearly related to wind forcing.
238 However, the scatter in the data indicates that other factors (such as spatial and temporal
239 variation in the instantaneous wind field, changes to fetch, drag, and water depth and variation
240 in ocean swell) influence the average hourly wave climate.

241
242 These factors produce a time history of wave climate that often deviates significantly from the
243 linear relationship. As shown in Fig. 6a, a decrease in wind velocity from $98 \text{ m}^2/\text{s}^2$ to 76
244 m^2/s^2 between $t=13$ hours and $t=15$ hours ($\sim 23\%$ decrease in energy) is correlated with a
245 non-linear decrease in the 20 minute mean square wave energy from $0.051 \text{ m}^2/\text{s}^2$ to 0.028
246 m^2/s^2 (45% decrease in energy). Similarly, between hour 20 and hour 21 the wind velocity
247 measured at the Richmond Field station was halved from 9.3 m/s to 4.7 m/s. This sudden
248 change in wind forcing causes a corresponding decline in the 20 minute mean square energy
249 of locally generated wind-waves from a maximum of $0.06 \text{ m}^2/\text{s}^2$ (rms velocity of 0.24 m/s) to

250 a maximum of $0.01 \text{ m}^2/\text{s}^2$ (rms velocity of 0.15 m/s) two hours later (figure 6a). Though a
251 linear model (e.g. Fig. 6c) predicts a factor 4x decrease in wave energy, the actually measured
252 wave energy decreases by a factor of 6x. This greater than expected decrease suggests that
253 other factors affect wave heights (e.g., water depth or tidal flow), and that variability in the
254 wind-field at periods of less than 1 hour may be important.

255
256 The sensitivity of wave energy to changes in wind climate is correspondingly reflected in the
257 measured SSC (figure 6b). Increases in SSC concentration coincide with increases in wind
258 energy (e.g., at $t=11$ hours and $t=19$ hours), while decreases in SSC correlate with decreases
259 in wind energy (e.g., at $t=15$ hours and $t=30$ hours). During periods of onshore wind (data
260 during the period of offshore wind from $t=55$ hours to $t=88$ hours are omitted), the
261 correlation between hourly averaged wind wave energy and hourly averaged SSC is $R^2 =$
262 0.41. When selected periods of anomalous SSC are removed (hours 19-21, 35-41 and 89), the
263 correlation is increased to $R^2=0.58$ and a reasonably linear trend is observed (see Fig. 6d).

264
265 The sensitivity of the regression in Fig. 6d to omitting data and the scatter around the linear
266 trend again points to the complexity and variability of the hydrodynamic forcing and sediment
267 dynamics. However, because the correlation between tidal velocity and SSC is insignificant
268 ($R^2 = 0.23$), other processes besides wind-waves and tidal currents must control the variation
269 of SSC (particularly during the times omitted in the analysis). These processes are the focus
270 of the following sections (section 3.3 and 3.4).

271
272 Note that winds directed offshore (blowing from North to South) may also cause elevated
273 SSC. For example, moderate offshore winds of 3-4 m/s during the ebb of tide 6 and flood of
274 tide 7 produce negligible wind-wave energy (see Fig. 5) and hence no local erosion.
275 However, the large SSC during the flood of tide 7 suggests that offshore wind is nonetheless
276 important, as it likely produces waves and erosion in subtidal areas and results in a larger SSC
277 signal than either the flood of tide 6 and tide 8, when offshore wind-forcing is much smaller
278 (see Fig. 4). By contrast, offshore winds during the ebb of tide 6 do not cause any erosion
279 upstream (shoreward) of the instruments, and no significant increase in SSC occurs. Note
280 that tidal velocities are slightly larger during the flood of tide 7 than either the flood of tide 6
281 or tide 8 (0.11 m/s vs. 0.07-0.08 m/s), and may also contribute to differences in offshore
282 erosion and advection during these flood tides. Finally, ocean swell forcing is larger during
283 the flood of tide 7 than during either the ebb of tide 7 or tide 8 (see Fig. 5), and may also
284 contribute to differences in SSC.

285
286

287 **3.3 Effect of Seiching on SSC**

288

289 To investigate the effect of seiching on SSC, we display the near bed 1-minute mean velocity
290 and SSC between $t=36.5$ hours and $t=40.5$ hours in Fig. 7a and Fig. 7b. Variations in
291 velocity and SSC at a period of 500-1000 seconds occur through-out this period, and serve to
292 increase the longer term mean SSC (e.g., tidal mean). Interestingly, a persistent asymmetry
293 occurs between SSC and the phase of the seiche, with the largest sediment concentrations
294 generally occurring when the seiche velocity is shoreward (shaded dark). This is clearly
295 observed in the scatter plot of the 1-minute mean velocity vs. the 1 minute mean SSC (Fig.
296 8c) during this 4 hour span. For mean, near bed velocities less than -0.05 m/s, near bed SSC
297 is restricted to a narrow band around 0.1 kg/m^3 . For velocities between -0.05 m/s and 0.15
298 m/s, SSCs trend upwards from 0.1 kg/m^3 to as much as 0.5 kg/m^3 .

299

300 Clearly, the stress exerted by the 1-minute mean flow cannot explain the observed sediment
301 concentration, since a mean velocity of zero m/s (mean stress = 0 N/m²) results in larger
302 sediment concentrations than an ebb velocity of 0.15 m/s. A possible explanation is that
303 sediment is being resuspended by the ejection of sediment off of bedform ripples as the fluid
304 reverses direction (e.g., Sleath & Wallbridge, 2002). Variation in the frequency of ejection
305 over a seiche would then produce the observed behaviour (Talke, 2005). Other explanations
306 include settling lag effects or lateral interaction with turbid channel water.

308 **3.4 Frontal processes**

309
310 While elevated SSC is often correlated with local wave action (e.g., the range of times
311 described in Fig. 6d, such as the flood of tide 5), examples of short duration (~ 30 minutes),
312 high concentration events that are decoupled from the local wind climate occur during the ebb
313 of tide 2 and the flood of tide 4, 6, and 8 (see Fig. 3 and Fig. 4). Such pulses of SSC, termed
314 the ‘turbid tidal edge’, are often observed on tidal flats (Dyer et al., 2000) and are attributed to
315 local erosion from tidal currents (e.g., Pritchard & Hogg, 2003). However, the small
316 maximum tidal currents of 0.07 m/s – 0.11 m/s during most of the experiment result in small
317 shear stresses of 0.015 N/m² to 0.03 N/m² (using the quadratic friction law with a drag
318 coefficient of 0.0025, an order of magnitude often found in coastal environments (e.g., Green
319 & McCave, 1995) and used in models (e.g., Roberts et al., 2000), which are unlikely to cause
320 local erosion. Moreover, the large rise in SSC often occurs as wind energy decreases (e.g.
321 ebb of tide 2 and flood of tide 4), and hence does not follow the linear relationship suggested
322 between SSC and wind (Fig. 6). In the absence of wind forcing, the turbid tidal edge still
323 occurs, despite the minimal local forcing (e.g., flood of tide 6 and tide 8).

324
325 A common feature of all the turbid pulses is that they coincide with sharp rises or falls in
326 salinity. Using the approximation that $ds/dx \sim ds/dt/U$ (where s = salinity and U = tidal
327 velocity), we estimate that the turbid pulse (> 0.9 kg/m³) and salinity decrease (22.5 psu to ~ 1
328 psu) between hour 20 and hour 21 coincides with salinity gradients of ~40 psu/km and that
329 the rise in turbidity (from 0.3 kg/m³ to 0.52 kg/m³) and salinity (+9.4 psu) at $t=26.25$ hours
330 over a 2 minute span implies a local gradient of ~ 800 psu/km. During the calmer periods of
331 tide 6 and tide 8, gradients of ~0.030 psu/m and 0.01 psu/m are advected past the sensors and
332 coincide with a factor ~ 5x increase in SSC (peak of 0.13 kg/m³ and 0.2 kg/m³, respectively).
333 Salinity gradients are larger during the flood, and are consistent with values observed in the
334 nearby subtidal channel by Ralston and Stacey (2005).

335
336 The sharp variations in sediment concentration and salinity observed during ebbing and
337 flooding periods suggests that a front influenced by freshwater runoff is moving past the
338 sensors. The pulse of SSC observed during the ebb of tide 2 and the flood of tide 3, tide 4,
339 tide 6, and tide 8 is consistent with a turbidity maximum formed at the interface of two bodies
340 of water in which longitudinal mixing is suppressed by strong horizontal density gradients.
341 This mechanism is described for the nearby channels by Ralston and Stacey (2005), and our
342 data suggests this process also occurs on the adjoining flats. The SSC in a front likely
343 consists of sediment eroded non-locally during the previous tidal period or at offshore (more
344 energetic) locations, and held in suspension by settling lag and turbulence effects (Ralston &
345 Stacey, 2007). Frontal processes govern the formation, dispersion, and time scale of the
346 pulses of SSC. While Ralston and Stacey (2005, 2007) describe a process occurring primarily
347 during flood tides after Low-Low-Water (LLW), our data suggests frontal processes can occur
348 during the ebb (e.g., tide 2) and after High-Low-Water (HLW) given sufficient freshwater
349 discharge (e.g., tide 6).

350
351

352 3.5 Sediment fluxes

353

354 In this section we investigate the sediment flux occurring over a tide at different time scales.
355 Combining the effect of locally driven wind waves and ocean swell together, we split the
356 measured velocity $V(t)$ and sediment concentration $C(t)$ into wave, seiche, tidal, and residual
357 (tidally averaged) components,

358

$$359 \quad C = C_{residual} + C_{tide} + C_{seiche} + C_{wave}, \quad (1)$$

360

$$361 \quad V = V_{residual} + V_{tide} + V_{seiche} + V_{wave}. \quad (2)$$

362

363 Velocity is decomposed along the North-South axis, which corresponds to the down-slope
364 direction and the primary direction of both wave and tidal forcing. Using the function f for
365 either the measured sediment concentration, C , or velocity, V , we decompose the measured
366 signal using bin-averages over the time scales T , N , and M ,

367

$$368 \quad f_{residual} = \frac{1}{T} \sum_{t=0}^{t=T} f(t) \Delta t, \quad (3)$$

369

$$370 \quad f_{tidal}(t) \Big|_{t=N(i-1)}^{t=iN-\Delta t} = \frac{1}{N} \sum_{t=N(i-1)}^{t=iN} (f(t) - f_{residual}) \Delta t, \quad i = 1, 2, \dots, T/N \quad (4)$$

371

$$372 \quad f_{seiche}(t) \Big|_{t=j(M-1)}^{t=jM-\Delta t} = \frac{1}{M} \sum_{t=j(M-1)}^{t=jM} (f(t) - f_{residual} - f_{tidal}) \Delta t, \quad j = 1, 2, \dots, T/M \quad (5)$$

373

$$374 \quad f_{wave}(t) = f(t) - f_{residual} - f_{tidal} - f_{seiche}. \quad (6)$$

375

376 The time increment Δt is the sampling period of 1/8 second. These decompositions result in
377 histograms of velocity and SSC with time increments of T , N , or M (Eqs. 3, 4, and 5,
378 respectively). The residual time scale for an intertidal flat is the time of immersion, T , which
379 we estimate as an integer number of 10 minute measurement bursts. We define the tidally
380 varying time scale N to be 1800 seconds (30 minutes), and the variability of the seiche scale
381 M to be 60 seconds (1 minute). These time scales correspond to periods of low energy in the
382 power spectrum of velocity, as defined by the frequencies 1/1800 Hz and 1/60 Hz in figure 5.
383 While some unsteadiness from lower frequencies is contained in higher frequency
384 components, (e.g., the tidal signal varies somewhat over 30 minutes and enters f_{seiche}), this
385 variability is small compared to the higher frequency variability (e.g., the seiche). Note that
386 the number T/N is rounded up to the nearest integer. When T/N is not an integer number, the
387 averaging time of the last bin is defined by the time period of the remainder. In practice, this
388 means that N is equal to 10 or 20 minutes for the last bin in some tidal periods, and may result
389 in some truncation of the seiche signal.

390

391 Assuming that diffusive fluxes are small, the average sediment flux $\Phi_{SSC} = \frac{1}{T} \int_0^T CV dt$ over a

392 period of immersion T at one point in the water column is then:

393

$$394 \quad \Phi_{SSC} = \frac{1}{T} \int_0^T (C_{wave} V_{wave} + C_{seiche} V_{seiche} + C_{tidal} V_{tidal} + C_{residual} V_{residual} + \Phi_{cross-terms}) dt. \quad (7)$$

395

396 The cross-terms are extremely small when integrated over the time period T , and are typically
397 less than $10^{-12} \text{ kg m}^{-2} \text{ s}^{-1}$ (see the electronic supplement for additional discussion).

398

399 The sediment fluxes occurring during tides 1-4 and tides 5-8 are shown in Fig. 8a and Fig 8b.
400 Positive values of flux denote onshore transport, while differences in y-axis scaling between
401 Fig. 6a and Fig. 6b reflect the order of magnitude larger fluxes during tides 1-4. The tidally-

402 averaged, residual flux of sediment ($\frac{1}{T} \int_0^T C_{residual} V_{residual} dt$) is directed offshore during tides 1-4

403 (average of $-5.4 \cdot 10^{-3} \text{ kg/m}^2/\text{s}$) but nearly vanishes during tides 5-8 ($6.5 \cdot 10^{-6} \text{ kg/m}^2/\text{s}$). Flux

404 from tidally varying processes, $\frac{1}{T} \int_0^T C_{tidal} V_{tidal} dt$, is offshore during tides 1-4 (average of -

405 $4.0 \cdot 10^{-4} \text{ kg/m}^2/\text{s}$) and onto the flat for tides 5-8 ($5.5 \cdot 10^{-4} \text{ kg/m}^2/\text{s}$). The flux of SSC at the

406 seiching frequency, $\frac{1}{T} \int_0^T C_{seiche} V_{seiche} dt$, is always directed onshore, and accounts for 14 percent

407 of the total flux during tides 1-4, but less than 1% of the flux during tides 5-8. Fluxes at the

408 wave frequency ($< 1/60 \text{ Hz}$) are small but non-negligible during tides 3-4. Because no

409 coherence is observed in the optical backscatter signal at wind-wave frequencies, these fluxes

410 may reflect transport due to lower frequency variability such as ocean swell or wind-wave

411 groups.

412

413 Overall, tidally-averaged, residual processes dominate net export of sediment during the

414 meteorological event of tides 1-4 (i.e., $\int_0^T CV dt < 0$) and tidally varying processes produce

415 onshore flux during the calmer period of tides 5-8 (i.e., $\int_0^T CV dt > 0$). Offshore sediment

416 fluxes during the meteorological event (tides 1-4) are an order of magnitude larger than the

417 onshore fluxes during the calmer period immediately afterwards (tides 5-8).

418

419 **4. Discussion**

420

421 In this section we discuss the physical mechanisms that produce fluxes during both the
422 meteorological event and afterwards.

423

424 **4.1 Residual, tidally averaged fluxes**

425

426 The dominance of tidally-averaged, residual fluxes during tides 1-4 is caused by order of

427 magnitude increase in $C_{residual}$ and $V_{residual}$ above non-event conditions (e.g., tides 5-8). Fig. 9

428 shows that during the meteorological event, residual flow off the flat increases from ~ -0.01

429 m/s at the beginning of the meteorological event (tide 1) to a maximum of -0.075 m/s during

430 tide 2. By comparison, the tidally-averaged velocities after the meteorological event vary

431 from 0.001 - 0.008 m/s . Similarly, tidally averaged sediment concentrations during the

432 meteorological event (0.11 - 0.19 kg/m^3) are much larger than sediment concentrations

433 afterwards ($0.02 - 0.05 \text{ kg/m}^3$). The combination of elevated sediment concentrations and
 434 increased residual flows causes large fluxes of sediment off the flat, particularly for tides 2, 3,
 435 and 4. During the calm period after the meteorological event, tidally averaged fluxes are
 436 correspondingly decreased; moreover, because the direction of flux is positive during tide 5
 437 and tide 7 but negative during tide 6 and tide 8, the integrated net flux over the post-event
 438 period is further reduced.

439

440 During the meteorological event between April 11th and April 13th, many factors may work
 441 together to create the residual flow pattern. The large salinity variations observed during this
 442 time period (see Fig. 3) indicate an influence of freshwater runoff from the local water shed.
 443 Wind stress also produces circulation patterns, as evidenced by water level set-up and its
 444 release during tides 1-5. The large salinity gradients likely drive gravitational circulation,
 445 which was found by Ralston and Stacey (2005) to produce a near-bottom inflow on the order
 446 of $0.01-0.02 \text{ m/s}$ over the shoal of our experimental site. Finally, the diurnal inequality in
 447 water level that occurs during tides 1-4 results in residual, tidally averaged currents.

448

449 The tidally averaged increase in SSC during tides 1-4 is primarily a result of the increased
 450 wave forcing, as suggested by the regressions in Fig. 6. However, seiching motions also
 451 appear to drive increases in tidally averaged SSC (see section 3.3). The more rigorous mixing
 452 during periods of large wind-waves also keeps sediments in suspension during slack tides,
 453 hence reducing the deposition (removal) of sediments. Combined with the offshore flow of
 454 water near the bed, sediment is exported from the flat to deeper offshore waters.

455

456

457 **4.2 Tidal Time Scale**

458

459 Sediment flux due to tidally varying processes is controlled by asymmetries in SSC and
 460 velocity over a tidal period. We investigate the factors influencing net flux at the tidal time
 461 scale by decomposing the SSC and velocity measurements into symmetric and asymmetric
 462 components

463

$$464 \quad C_{tidal} = C_{base} + C' \quad (8a)$$

465

$$466 \quad V_{tidal} = V_{base} + V' \quad (8b)$$

467 where C_{base} is an even (symmetric) function and V_{base} is an odd function with respect to the
 468 midpoint of the period of immersion ($T/2$), and C' and V' are deviations from the
 469 symmetrical function over the tidal period. Using our data, we define the even component of
 470 SSC around $T/2$ as follows:

471

$$472 \quad C_{base}(t) = C_{tidal}(t), \quad t < T/2 \quad (9)$$

473

$$474 \quad C_{base}(t) = C_{tidal}(T-t), \quad t > T/2$$

475

476 The odd component of velocity is defined similarly:

477

$$478 \quad V_{base}(t) = V_{tidal}(t), \quad t < T/2 \quad (10)$$

479

$$480 \quad V_{base}(t) = -V_{tidal}(T-t), \quad t > T/2$$

481
 482 Using these definitions, we find that the tidally integrated flux of SSC at the tidal time scale
 483 can be rewritten as,
 484

$$485 \quad \frac{1}{T} \int_0^T C_{tidal} V_{tidal} dt = \underbrace{\frac{1}{T} \int_0^T C_{tidal} V' dt}_{\Phi_{V'}} + \underbrace{\frac{1}{T} \int_0^T V_{base} C' dt}_{\Phi_{C'}}, \quad (11)$$

486
 487 where we have used the observation that the integral of the product of even and odd functions
 488 vanishes over the time period T , i.e., $\int_0^T (C_{base} V_{base}) dt = 0$. Hence, asymmetries in velocity (V')
 489 and SSC (C') over a tidal period are required to produce sediment fluxes $\Phi_{V'}$ and $\Phi_{C'}$,
 490 respectively (see Eq. 11).
 491

492 Fig. 10 shows the magnitude of the sediment fluxes $\Phi_{V'}$ and $\Phi_{C'}$ over tides 1-8. During tides
 493 1-3, both components of flux are on the same order of magnitude. By contrast, the $\Phi_{V'}$ term
 494 nearly vanishes during tides 5-8 and the tidally varying fluxes are dominated by asymmetries
 495 in SSC between the flood and the ebb.
 496

497 To understand why the shift to $\Phi_{C'}$ dominance occurs in tides 5-8, we investigate the tidal
 498 variation of SSC (Fig. 11a and Fig. 12a), velocity (Fig. 11b and 12b) and the product
 499 $C_{tidal} V_{tidal}$ (Fig. 11c and Fig. 12c) during tides 1-4 (Fig. 11) and tides 5-8 (Fig. 12). Onshore
 500 velocity and sediment flux are shaded dark and defined as (+), whereas offshore sediment flux
 501 and velocity are shaded light and defined as (-). Similarly, positive deviations from the tidal
 502 averaged SSC are shaded dark (+) and negative deviations are shaded light and defined as (-)
 503 (see Eq. 5). The function C_{base} is depicted in Fig. 11a and Fig. 12a and the function V_{base} is
 504 depicted in Fig. 11b and Fig. 12b.
 505

506 During the meteorological event, both SSC and velocity are quite asymmetric, as can be
 507 observed by the differences between the measured tidal variation (C_{tidal} and V_{tidal}) and the
 508 hypothetical symmetric functions C_{base} and V_{base} . While SSC remains asymmetric over a
 509 tidal period during tides 5-8, the flow velocity is relatively symmetric (as shown by the
 510 relatively good agreement between V_{base} and V_{tidal}).
 511

512 4.2.1 Factors producing asymmetry

513
 514 The asymmetric tidal variation in flow velocity during the meteorological event, V' , is caused
 515 both by the diurnal inequality in tides and by events such as freshwater discharge and wind
 516 induced circulation and setup/set-down. For example, the diurnal inequality results in small
 517 tidal currents during the ebb of tide 1 and flood of tide 2, and contributes to an onshore
 518 $\Phi_{V'}$ during tide 1 and an offshore $\Phi_{V'}$ during tide 2 (see Fig. 10). The setup caused by wind
 519 also appears to prolong the flood tide during tide 2. Finally, the coincidence of freshwater
 520 discharge (as evidenced by salinity concentrations < 10 psu) and the release of water set-up
 521 due to decreasing wind at hour 20 cause large ebb currents. As the diurnal inequality
 522 diminishes and the freshwater discharge and setup disappear (particularly after tide 5), the
 523 asymmetric velocity profile becomes unimportant to the flux balance. Hence, unlike

524 modelling studies suggest (e.g., Ridderinkhof, 1998), asymmetries in velocity caused by over-
525 tides (e.g., the M₄ tide) do not appear to be important for fluxes at our site.

526

527 Two primary forcing mechanisms produce asymmetries of SSC over a tidal cycle at our site:
528 The turbid tidal edge (mediated by frontal processes) and the tidal variation in wind forcing.
529 In the absence of significant wind or wave activity (e.g., tide 6), the baseline asymmetry in
530 SSC is characterized by higher concentrations on flood tides than on ebbs due to the turbid
531 tidal front. These frontal pulses of turbidity are associated with strong salinity gradients,
532 occur over a short time scale ($\ll 1$ hour), and are usually largest during the flood tide (see
533 section 3.4). Variations in wind forcing cause tidal variations in wind-wave energy and
534 seiching (see Fig. 5) over time scales greater than an hour, and hence alter SSC (see section
535 3.2 and 3.3).

536

537 The tidal asymmetry in SSC due to wind forcing is most clearly observed by comparing tide 5
538 and tide 8. During the flood of tide 5, wind-driven waves produce a peak concentration of
539 $\sim 0.2 \text{ kg/m}^3$ above the tidal mean, which reduces over 1.5 hours as wind forcing subsides (see
540 Figs. 4 and 12). Because wind-wave energy is negligible during the ebb (see Fig. 5), SSC
541 does not increase much and a flood dominated SSC asymmetry (and onshore sediment flux)
542 occurs. By contrast, wind energy and wave energy are small during the flood of tide 8, but
543 increase during the ebb (see Fig. 4 and Fig. 5). As a result, SSC shifts above the tidal average
544 for 1.5 hours during the ebb of tide 8, producing a net offshore flux.

545

546 The effect of variable wind-forcing on asymmetries in SSC is not solely tied to local
547 variations in wind-driven waves. For example, seiching motions are much larger during the
548 flood of tide 4 than during the ebb, likely due to the decrease in wind forcing (and release of
549 setup) that occurs after hour 33 (see Fig. 3 and Fig. 5). These seiching motions not only
550 increase the magnitude of SSC at the seiche frequency (see Fig. 7), but also increase the
551 tidally varying SSC (e.g., between hour 38-40 in Fig. 11). Similarly, the decrease in wind
552 during the ebb of tide 2 is correlated with large ebb currents that can erode sediment.
553 Offshore (southwards directed) wind may stir offshore, subtidal sediments (through wave
554 action) which are transported shoreward during the flood, and cause a flood dominated
555 asymmetry in SSC over a tidal period (e.g. tide 7; see section 3.2). Finally, ocean swell
556 forcing is larger during the ebb of tide 5 and the flood of tide 7 than the corresponding flood
557 and ebb, respectively, and may also contribute to asymmetries in SSC.

558

559 **4.2.2 Effects of Phasing and Time Scales**

560

561 The net effect of asymmetries in velocity (V') and SSC (C') depends on their relative phasing
562 with C_{tidal} and V_{base} and on their respective magnitudes and time-scales of variation.
563 Instantaneous fluxes of SSC at the tidal time scale are maximized when large SSC is
564 correlated with large advective velocities. As shown in Fig. 11 and Fig. 12, examples of such
565 events are found during the ebb of tide 2 (hour 20) and the flood of tide 1 (hour 2) and 5 (hour
566 51-53). Much smaller fluxes, however, occur when large SSC corresponds with small tidal
567 velocities (e.g., hour 35), or when maximum tidal velocities occur at small SSC (hour 70 or
568 hour 84).

569

570 Because of differing time scales and timing, turbid tidal fronts and wave induced turbidity
571 events interact differently with V_{base} in Eq. 11. Turbid pulses during the flood are often higher
572 in magnitude than the corresponding increase in SSC during the ebb (see tide 6 and tide 8 in
573 Fig. 12), and drive onshore flux in calm conditions (e.g. tide 6). However, the time-scale over

574 which the turbid pulse acts is small (~ 30 minutes) compared to wave induced turbidity
575 events, which generally occur over time periods of greater than 1 hour (see flood of tide 5 and
576 ebb of tide 8, for example). Hence, fluxes from the relatively small SSC during the ebb of
577 tide 8 (Fig. 12), which is integrated over 1.5 hours, outweighs the short but intense turbidity
578 front which is integrated over 30 minutes. The effect of the differing time scales is amplified
579 by the timing of the front and the wind event. The front during the flood of tide 8 occurs at a
580 non-peak flood velocity (0.053 m/s vs. 0.083 m/s at the maximum), while the much smaller
581 maximum SSC during the ebb of 0.08 kg/m³ occurs at the nearly the maximum ebb velocity
582 (0.081 m/s). Because wind-events are longer, they are more likely to coincide with the
583 maximum tidal velocity and therefore produce large sediment fluxes.

584

585 4.3 Time Scales of Wind and Swell

586

587 As observed in the previous section, the timing of wind events relative to the phase of the tide
588 modifies the net flux onto or off of the flat. Two basic conditions may occur. First, the wind
589 wave event may last over the entire tidal period, as occurs during most of tide 2 during the
590 meteorological event. On the other extreme, wind events may occur entirely during the flood
591 (tide 5) or during the ebb (tide 8). To understand the likelihood that a wind event will be
592 biased towards either the flood or ebb, we analyze wind data from the Richmond Field Station
593 for the years 1999-2005. We define an event to be the time period over which sustained
594 winds are greater than 5 m/s, which is a standard deviation from the long term mean of 3.2
595 m/s and is also the order of magnitude for which sediment resuspension occurs on other
596 intertidal flats (de Jonge and van Beusekom, 1995, Christie et al., 1999, Dyer et al. 2000).
597 Two events that are separated by only 1 hour are combined into one event period, to allow for
598 randomness in the wind field during a contiguous event. For comparison, we also analyze the
599 significant wave height (average of top 1/3 measured wave amplitudes per hour) measured at
600 an offshore buoy (NDBC buoy 46026) for an estimate of offshore swell. Again, we define an
601 event as a standard deviation from the average, which is 2.8 m (mean significant wave height
602 = 2.0 m). Though ocean swell rarely dominates the energy budget at this site, Fig. 5 shows
603 that ocean swell provides an important contribution to the total forcing. Thus, the time scales
604 of ocean swell provide an interesting contrast to locally driven wind waves.

605

606 Results in Fig. 13 show that the most likely time scale of both a wind event and ocean swell
607 event is 1 hour (26% and 28%, respectively). Thus, as confirmed by the spectral analysis of
608 velocity (see Fig 5), both ocean swell and wind waves are highly likely to occur over only a
609 portion of the tide: ~ 51% of wind events are 3 hours or less, while ~ 54% of offshore swell
610 events are 5 hours or less. Indeed, 90% of wind events have a time period of less than 12
611 hours, the time scale of a tide. By contrast, 28% of offshore swell events exceed the time
612 scale of a tidal period.

613

614 The frequency distribution of wind and ocean swell events suggests that the strong
615 dependence of tidally integrated sediment flux to variations in wind and waves are a long-
616 term characteristic of this intertidal flat, and not just an artefact of this experiment. Changes
617 in wind forcing and hence sediment flux are observed both within a tidal phase (e.g., during
618 the ebb of tide 2 between hour 20 and 21) and between tidal phases (e.g., the flood and ebb of
619 tide 5 or tide 8). As a result, the phasing and duration of wind and wave events relative to the
620 local tidal forcing is an important factor in the net sediment flux. Hence, the assumption that
621 wind forcing is constant over a tidal period in models of sediment transport (e.g.,
622 Ridderinkhof, 1998, Roberts et al., 2000, Waeles et al., 2004), may need to be examined.

623

624 **5. Conclusions**

625
626 Field observations of hydrographic parameters and sediment concentration on an intertidal
627 flat show that multiple frequencies of forcing contribute to the flow field, including locally
628 driven wind-waves, ocean swell, intra-tidal seiching motions (500-1000 second period), tidal
629 flows, and sub-tidal variation such as freshwater discharge. Because the median time scale of
630 wind and swell events is small (3 hours and 5 hours, respectively), wave and seiching motions
631 (and hence SSC) are often asymmetrically distributed between ebb and flood. Precipitation
632 from a meteorological event leads to freshening and the formation of a sharp salinity front
633 that is advected past the sensors during the flood and ebb. Sediment is trapped at the salinity
634 front, and is observed at the sensors as a short (~ 30 minutes) but intense increase in SSC.

635
636 Sediment is exported during a meteorological event primarily due to wind driven and
637 freshwater forcing. Tidally averaged fluxes of SSC dominate and are marked by an order of
638 magnitude increase in both the residual circulation (offshore) and tidally-averaged sediment
639 concentration. The enhanced residual circulation is likely driven by wind and freshwater
640 forcing, while increases in SSC are primarily driven by local wind-waves and seiching.
641 Tidally varying processes (such as wind forcing and frontal dynamics) either amplify (tide 2)
642 or diminish (tide 4) the net sediment fluxes during the meteorological event by producing
643 asymmetries in both the tidal velocity and the tidal profile of SSC. Net sediment fluxes at the
644 seiche frequency are always onshore due to a bias in SSC with respect to the seiche period,
645 and occur primarily during the meteorological event.

646
647 After the meteorological event, both tidally averaged wind and freshwater forcing relax and
648 the dominant contribution to sediment flux is made by tidally varying processes. In
649 particular, the flood tide is marked by elevated turbid fronts, both from onshore wind (tide 5),
650 offshore wind (tide 7) and salinity driven frontal processes (tide 6 and tide 8). By contrast,
651 salinity decreases more gradually during the ebb and little erosion or trapping of SSC occurs.
652 As a result of this asymmetry in SSC, sediment flux is generally onshore. However, moderate
653 onshore wind of 3-4 m/s during an ebb period (e.g., tide 8) is capable of producing significant
654 increases to SSC and reversing the net sediment flux.

655
656 To conclude, sediment fluxes at an intertidal flat are controlled by periodic tidal forcing and
657 by event driven processes such as wind and freshwater discharge. The shifting influence of
658 wind and freshwater discharge over a period of days produces large, tidally averaged fluxes
659 during a meteorological event and produces the asymmetries necessary for sediment transport
660 at a tidal frequency. Over the time period considered, the phasing and duration of wind
661 events and freshwater discharge relative to the local tidal forcing greatly affect net sediment
662 flux.

664 **Acknowledgements**

665 Many thanks to David Ralston, Jon Fram, Deanna Sereno, Seungjin Baek, Shitao Xu, Kate
666 Hucklebridge, Josh Sharp, and Kurt Talke for logistical support during the experiment. The
667 research was funded by National Institutes of Health grant number P42ES0475 from the
668 National Institute of Environmental Health Sciences, and was completed with the funding of
669 LOICZ project 014.27.013 (Land Ocean Interaction in the Coastal Zone, funded by NWO-
670 ALW, the Netherlands Organization for Scientific Research). The authors thank the
671 anonymous reviewers for their helpful and constructive criticism.

672
673

674 **References**

675

676 Andersen, T.J., M. Pejrup, 2001. Suspended sediment transport on a temperate, microtidal
677 mudflat, the Danish Wadden Sea. *Marine Geology*, **173**, 69-85.

678

679 Bassoullet, P., Hir, P.L., Gouleau, D., Robert, S., 2000. Sediment transport over an intertidal
680 mudflat: Field investigations and estimation of fluxes within the 'Baie de Marennes-Oleron'
681 (France). *Continental Shelf Research*, **20**, 1635-1653.

682

683 Black, K.S., 1998. Suspended Sediment Dynamics and Bed Erosion in the High Shore
684 Mudflat Region of the Humber Estuary, UK. *Marine Pollution Bulletin*, **37**, Nos. 3-7, 122-
685 133.

686

687 Christiansen, C., Vølund, G., Lund-Hansen, L.C., & J. Bartholdy, 2006. Wind influence on
688 tidal flat sediment dynamics: Field investigations in the Ho Bugt, Danish Wadden Sea.
689 *Marine Geology* **235**, 75-86.

690

691 Christie, M.C., Dyer, K.R., Turner, P., 1999. Sediment Flux and Bed Level Measurements
692 from a Macro Tidal Mudflat, *Estuarine, Coastal and Shelf Science* **49**, 667-688.

693

694 de Haas, H., Eisma, D., 1993. Suspended-Sediment Transport in the Dollard Estuary,
695 *Netherlands Journal of Sea Research*, **31** (1), 37-42.

696

697 de Jonge, V.N., van Beusekom, J.E.E., 1995. Wind and tide induced resuspension of
698 sediment and microphytobenthos from tidal flats in the Ems estuary. *Limnol. Oceanogr.* **40**:
699 766-778.

700

701 Dyer, K. R., 1998. The typology of intertidal mudflats. Black, K.S., Patterson, D.M., and
702 Cramp, A. (eds.), *Sedimentary Processes in the Intertidal Zone*. Geological Society, London,
703 Special Publications, **139**, 11-24.

704

705 Dyer, K.R., Christie, M.C., Feates, N., Fennessy, M.J., Pejrup, M., and van der Lee, W., 2000.
706 An Investigation into Processes Influencing the Morphodynamics of an Intertidal Mudflat, the
707 Dollard Estuary, The Netherlands: I. Hydrodynamics and Suspended Sediment. *Estuarine,*
708 *Coastal and Shelf Science*, **50**, 607-625.

709

710 Friedrichs, C.T., Aubrey, D.G. 1996 Uniform bottom shear stress and equilibrium hypsometry
711 of intertidal flats. In *Mixing in Estuaries and Coastal Seas* (ed. C. Pattiaratchi), Volume 50 of
712 *Coastal and Estuarine Studies*, pp. 405-429. American Geophysical Union.

713

714 Green, M.O., McCave, I.N., 1995. Seabed drag coefficient under tidal currents in the eastern
715 Irish Sea, *Journal of Geophysical Research*, **100**, C8, 16057-16070.

716

717 Janssen-Stelder, B., 2000. The effect of different hydrodynamic conditions on the
718 morphodynamics of a tidal mudflat in the Dutch Wadden Sea. *Continental Shelf Research* **20**,
719 1461-1478.

719

720 Kirby, R., 2000. Practical implications of tidal flat shape, *Continental Shelf Research*, **20**,
721 1061-1077.

722

- 723 Kornman, B.A., De Deckere, E.M.G.T., 1998. Temporal variation in sediment erodibility and
724 suspended sediment dynamics in the Dollard estuary. *In: Black, K.S., Paterson, D.M. and*
725 *Cramp, A. (eds.) Sedimentary Processes in the Intertidal Zone. Geological Society, London,*
726 *Special Publications, 139, 231-241.*
- 727
728 Le Hir, P., Roberts, W., Cazaillet, O., Christie, M., Bassoullet, P., Bacher, C., 2000.
729 Characterization of intertidal flat hydrodynamics. *Continental Shelf Research, 20, 1433-*
730 *1459.*
- 731
732 O'Brien, D.J., Whitehouse, R.J.S., Cramp, A., 2000. The cyclic development of a macrotidal
733 mudflat on varying timescales. *Continental Shelf Research 20, 1593-1619.*
- 734
735 Pritchard, D., Hogg, A.J., Roberts, W., 2002. Morphological modelling of intertidal mudflats:
736 the role of cross-shore tidal currents. *Continental Shelf Research, 22, 1887-1895.*
- 737
738 Pritchard, D., & A.J. Hogg, 2003. Cross-shore sediment transport and the equilibrium
739 morphology of mudflats under tidal currents. *Journal of Geophysical Research, 108, C10,*
740 *3313, doi:10.129/2002JC001570.*
- 741
742 Ridderinkhof, H. 1998. On the sensitivity of the large scale transport and distribution of fine
743 grained sediments in a tidal basin to the formulation of the erosion-sedimentation cycle. *In*
744 *Physics of Estuaries and Coastal Seas (eds. J. Dronkers & M. Sheffers), 145–153. Balkema.*
- 745
746 Ridderinkhof, H., Van der Ham, R., van der Lee, W., 2000. Temporal variations in
747 concentration and transport of suspended sediments in a channel-flat system in the Ems-
748 Dollard estuary. *Continental Shelf Research 20, 1479-1493.*
- 749
750 Ralston, D.K., 2005. Hydrodynamics and scalar transport in subtidal channels through
751 intertidal mudflats. PhD Thesis, University of California, Berkeley.
- 752
753 Ralston, D.K., Stacey, M.T., 2005. Longitudinal dispersion and lateral circulation in the
754 intertidal zone. *Journal of Geophysical Research-Oceans 110, C07015, 17 pp.*
- 755
756 Ralston, D.K., Stacey, M.T., 2007. Tidal and meteorological forcing of sediment transport in
757 tributary mudflat channels. *Continental Shelf Research, 27, 1510-1527.*
- 758
759 Roberts, W., Le Hir, P., Whitehouse, R.J.S., 2000. Investigation using simple mathematical
760 models of the effect of tidal currents and waves on the profile shape of intertidal mudflats.
761 *Continental Shelf Research 20, 1079-1097.*
- 762
763 Shi, Z., Chen, J.Y., 1996. Morphodynamics and sediment dynamics on intertidal mudflats in
764 China (1961-1994). *Continental Shelf Research, 16, No. 15, 1909-1926.*
- 765
766 Sleath, J.F.A., Wallbridge, S., 2002. Pickup from Rippled Beds in Oscillatory Flow. *Journal*
767 *of Waterway, Port, Coastal and Ocean Engineering, 128, 6, 228-237.*
- 768
769 Staats, N., de Deckere, E., Kornman, B., van der Lee, W., Termaat, R., Terwindt, J., de
770 Winder, B., 2001. Observations on suspended particulate matter (SPM) and microalgae in the
771 Dollard estuary, the Netherlands: Importance of late winter ice cover of the intertidal flats.
772 *Estuarine, Coastal, and Shelf Science, 53 (3) 297-306.*

773

774 Talke, S.A., 2005. An Investigation on the Hydrodynamics and Sediment Dynamics on an
775 Intertidal Mudflat on Central San Francisco Bay. *PhD Thesis*, University of California,
776 Berkeley.

777

778 Talke, S.A., Stacey, M.T., 2003. The influence of oceanic swell on flows over an estuarine
779 intertidal mudflat in San Francisco Bay, *Estuarine, Coastal, and Shelf Science* 58, 541-554.

780

781 Waeles, B., Le Hir, P., Jacinto, R. S. 2004 Modélisation morphodynamique cross-shore d'un
782 estran vaseux. *Comptes Rendus Geoscience* 336, 1025–1033.

783

784 Wright, S.A., Schoellhamer, D.H., 2004. Trends in the sediment yield of the Sacramento
785 River, California, 1957-2001. *San Francisco Estuary and Watershed Science* [online serial].
786 2, Issue 2, Article 2.

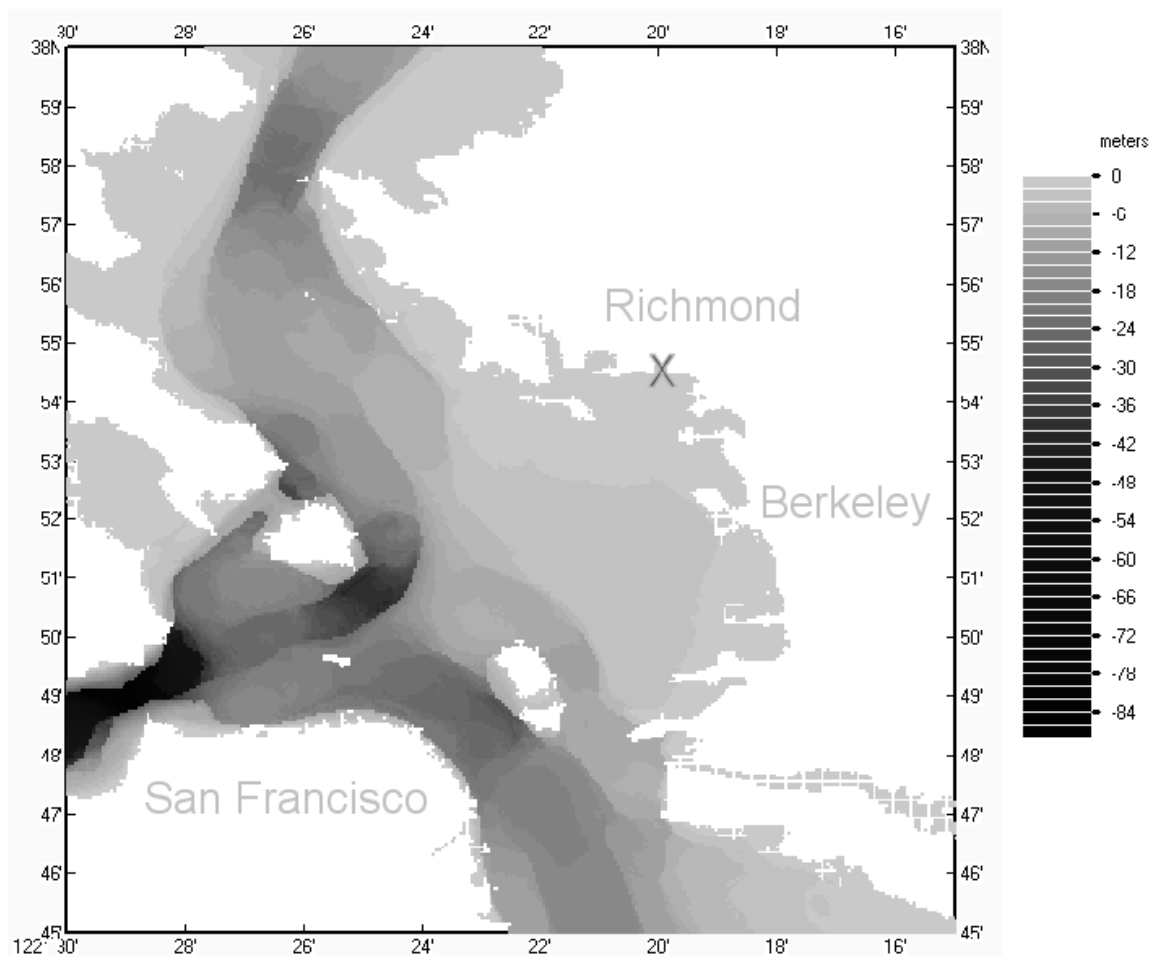
787

788 Yang, S.L., Friedrichs, C., Zhong, S., Ping-Xing, D., Zhu, J., Zhao, Q.Y., 2003.
789 Morphological Response of Tidal Marshes, Flats, and Channels of the Outer Yangtze River
790 Mouth to a Major Storm. *Estuaries*, 26, 1416-1425.

791

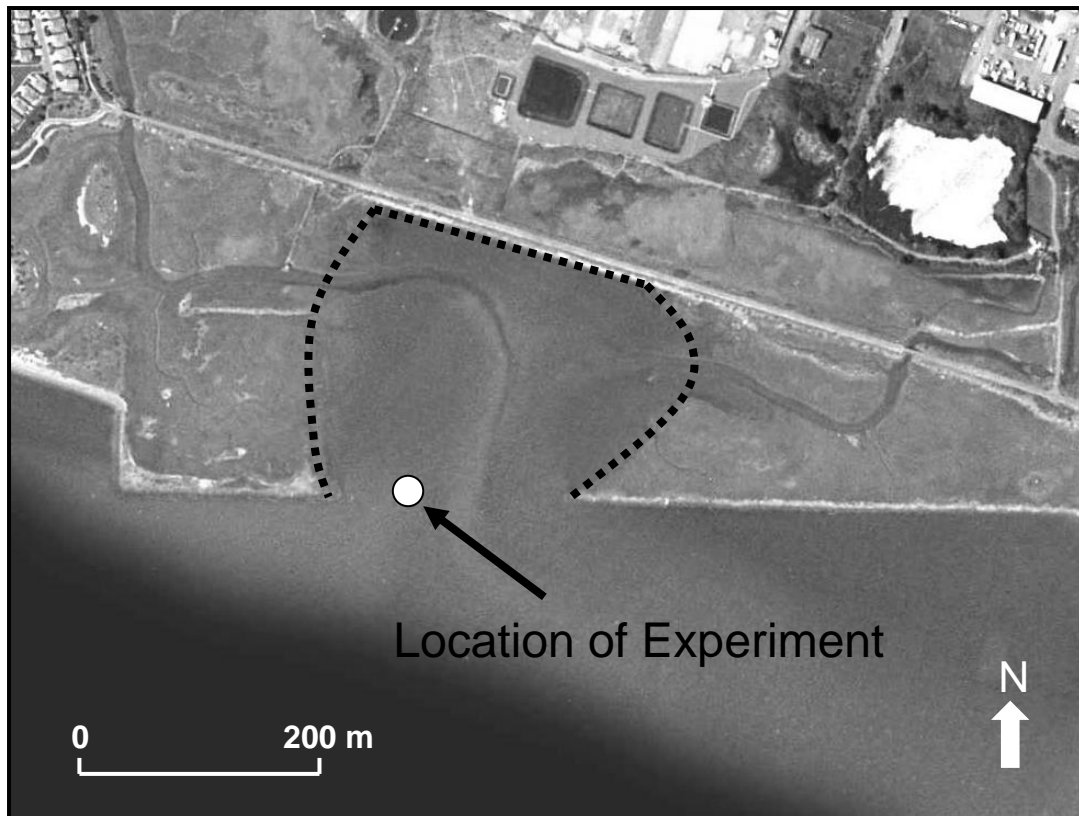
792 Figures

793



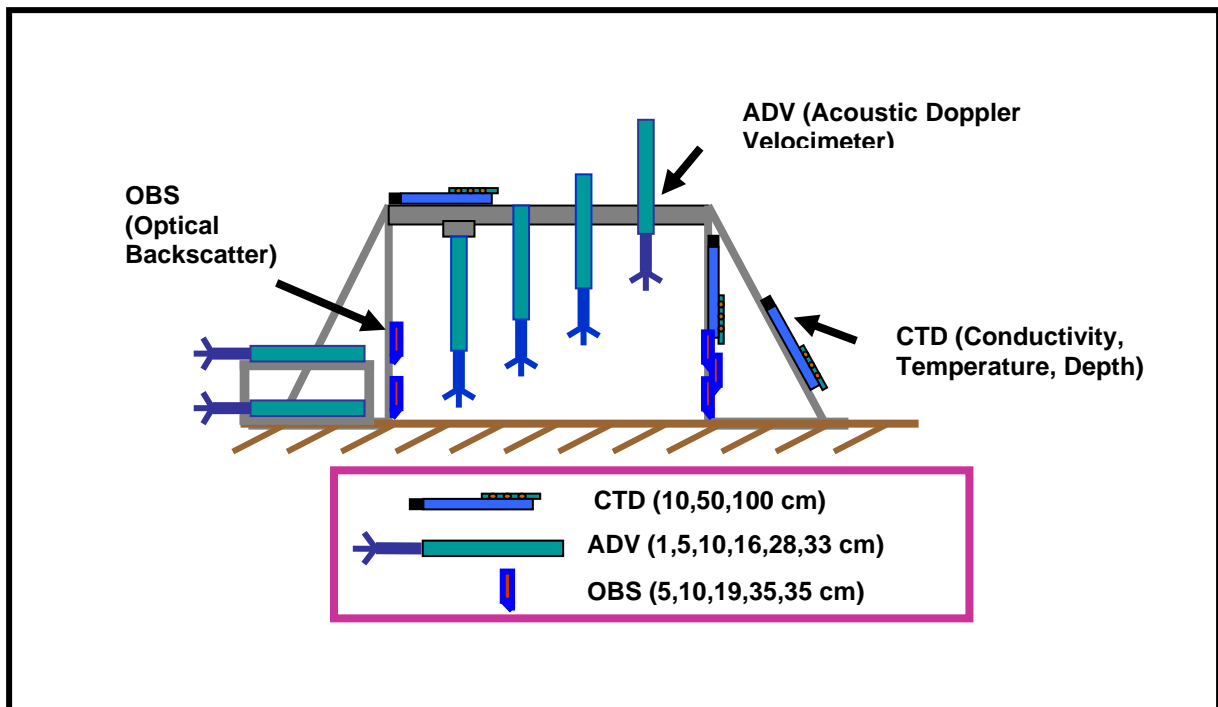
794

795 Figure 1-a: Location map of experiment in terms of latitude and longitude. The location of
796 the experiment is marked with an 'X'.



797
798
799
800
801
802

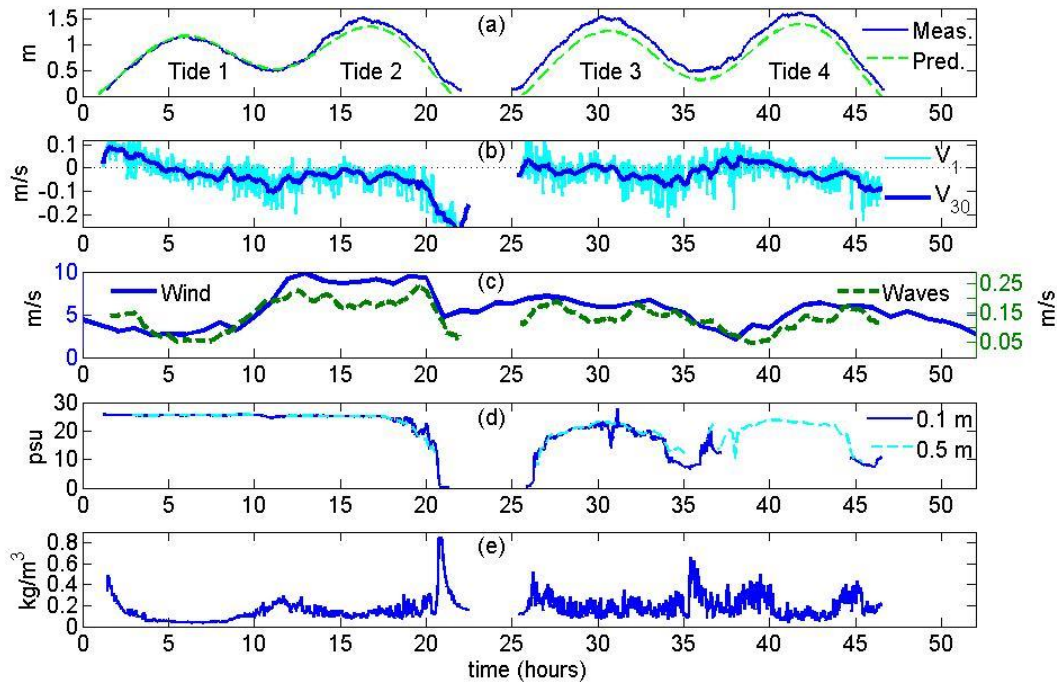
Figure 1b: Location of the instrument frame on the intertidal mudflat near the Richmond Field Station. The approximate borders of the mudflat with the intertidal marsh and the multi-use trail on the north side are denoted by the dotted line.



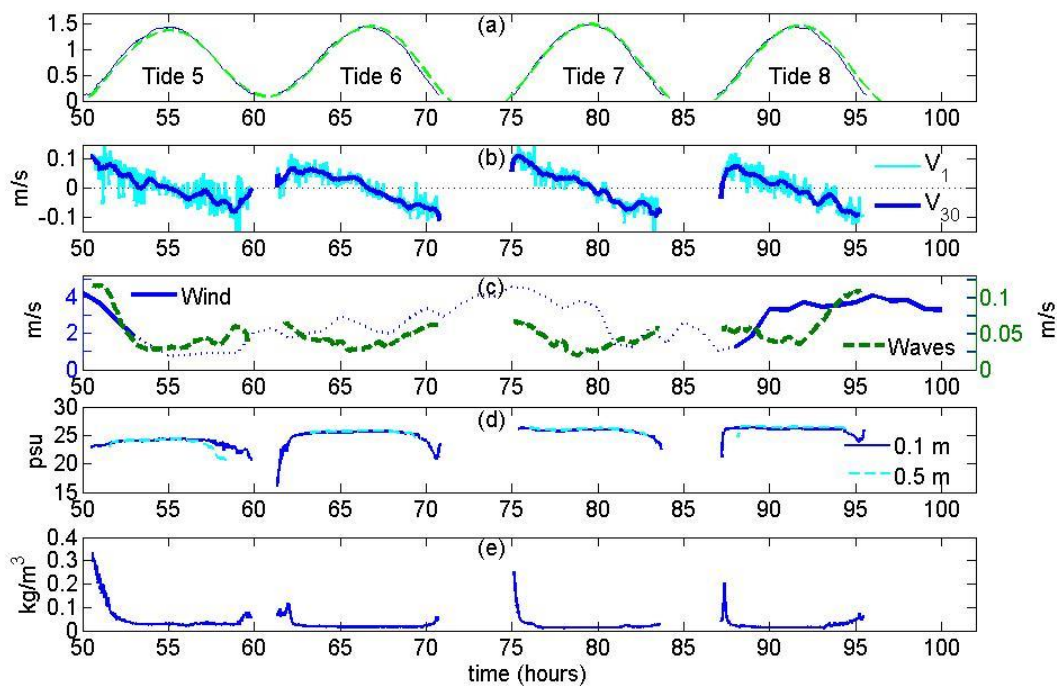
803
804
805
806
807
808
809

Figure 2: Depiction of experimental setup. Four downwards facing velocimeters were focussed 1 cm, 5 cm, 16 cm, and 28 cm from the bed, while two sideways pointed velocimeters were focused at 10 cm and 33 cm off the bed. Five optical backscatter and 3 CTD instruments were placed as depicted in the figure.

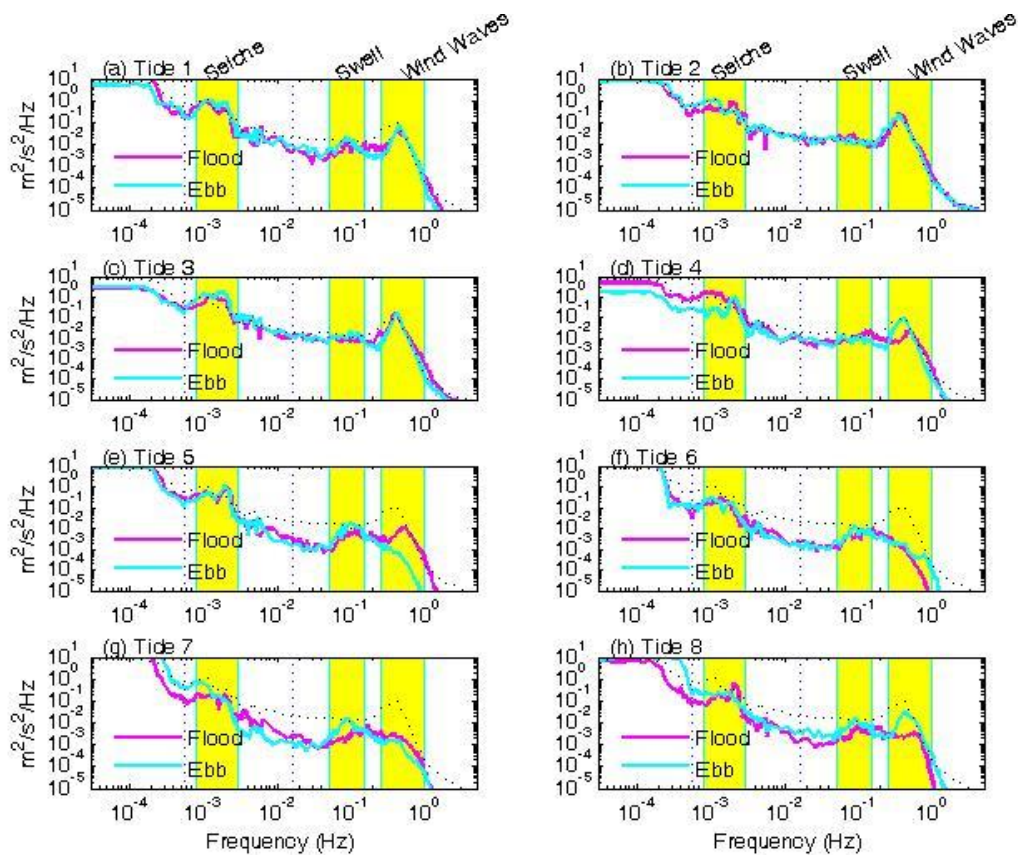
810



811
 812 Figure 3: Plots of (a) predicted and measured tides, (b) mean velocity, (c) wind and root-
 813 mean-square (rms) wave velocity, (d) salinity, and (e) suspended sediment concentration
 814 during a meteorological event (cold front). Zero hours refers to the start of the experiment at
 815 16:00 on April 11th, 2003. In (b), both a 1 minute block average (V_1) and a 30 minute
 816 moving average (V_{30}) are displayed, and zero velocity is marked with a dotted line. The rms wave
 817 velocity is calculated after removing the 1 minute mean velocity over blocks of 20 minutes.

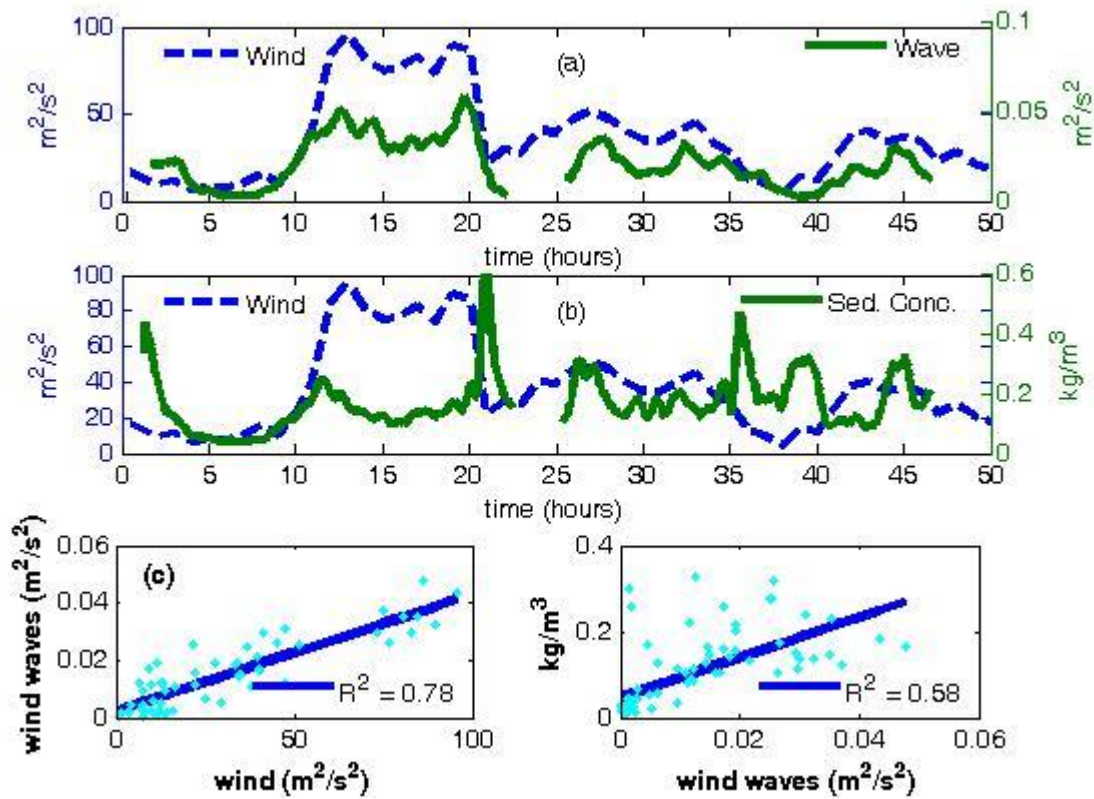


818
 819 Figure 4: Plots of (a) predicted and measured tides, (b) mean velocity, (c) wind and root-
 820 mean-square (rms) wave velocity, (d) salinity, and (e) suspended sediment concentration after
 821 a meteorological event (tides 5-8), following the same format as Fig. 3. Offshore wind
 822 velocity blowing from North to South in (c) is depicted with a dotted line.
 823



824
 825 Fig. 5: Comparison of the power spectrum of velocity between flood (dark shade) and ebb (light

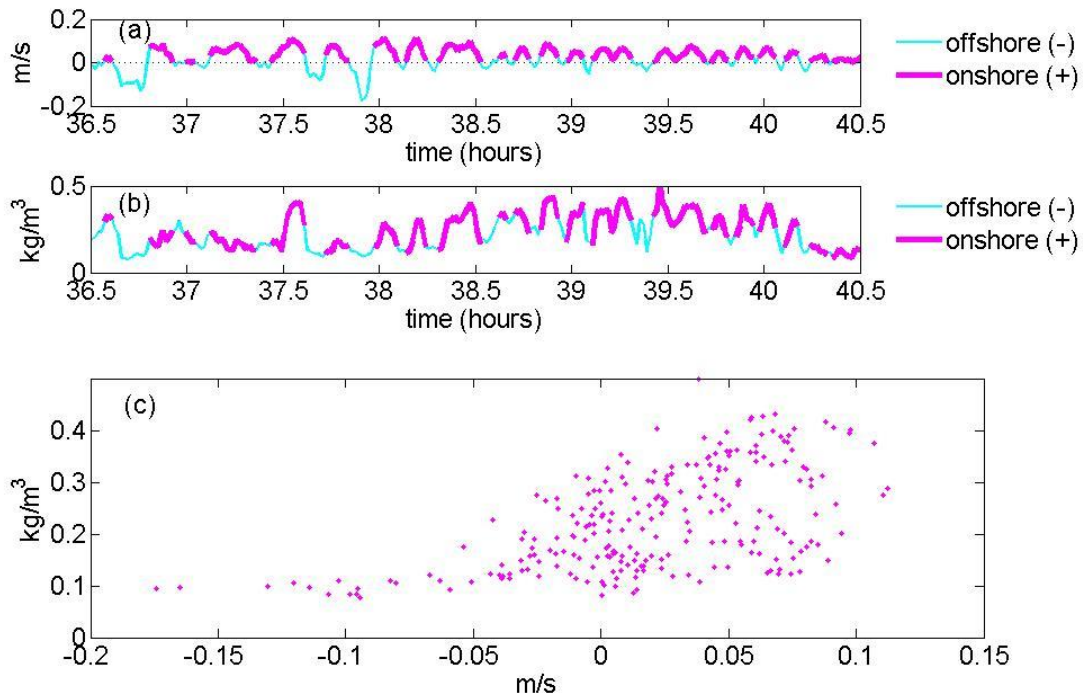
826 shade) over eight tidal periods. The seiche, ocean swell, and wind wave frequency bands are
827 shaded. For reference, the power spectrum during the ebb of tide 2 is presented as a dotted
828 line. The vertical dotted lines refer to frequencies of $1/60$ Hz and $1/1800$ Hz, and depict low
829 energy band.
830



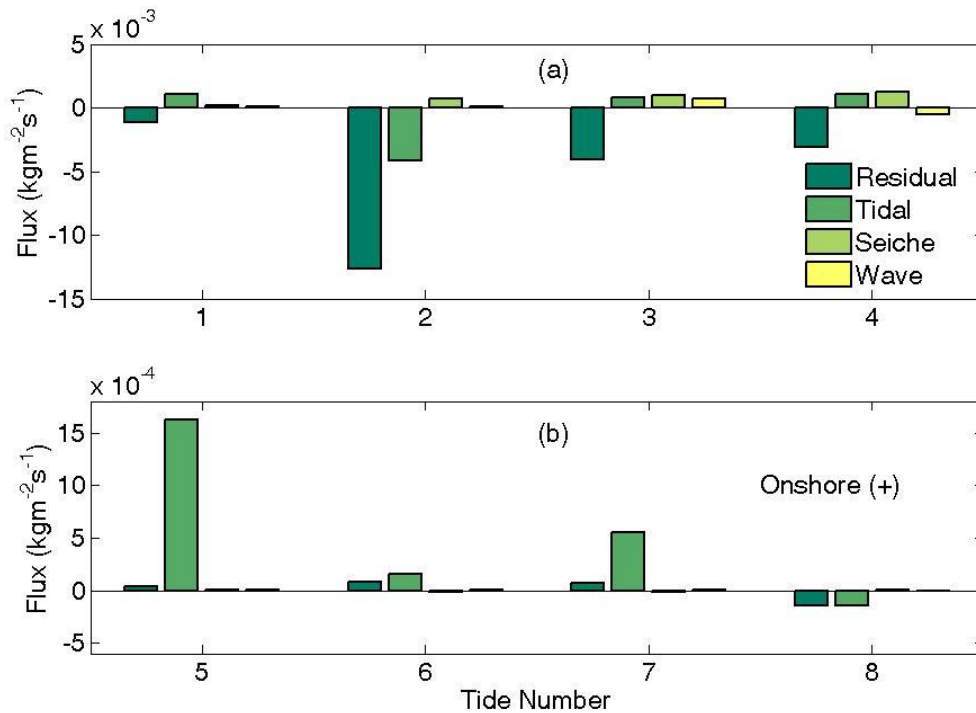
831
832
833
834
835
836
837
838
839
840
841
842

Figure 6: Evolution of wind energy (a,b), wave energy (a) and sediment concentration (b) vs. time, and scatter plots of hourly averaged wind wave energy vs. wind energy (c) and hourly averaged suspended sediment concentration vs. the hourly averaged wind wave energy (d). The sediment concentration in (b) is a 30 minute moving average. In (d), Sediment concentration measurements between hour 19-21, hour 35-41, and hour 89 are omitted because waves do not control sediment concentration values directly during this time. In addition, Wind energy between $t=55$ hours and $t=88$ hours is omitted because it is blowing towards the south (i.e., off the mudflat). Correlation of the line fit to data is given by the R^2 value.

843
844
845



846
847 Figure 7: Plot of the (a) 1 minute mean velocity, (b) 1 minute mean SSC, and a scatter plot
848 (c) of 1 minute mean SSC vs. 1 minute mean velocity over the time period $t=36.5$ hours to t
849 $= 40.5$ hours. Periods of onshore directed velocity are shaded dark in (a) and (b).
850 Measurements occurred at $O(0.1$ m) off the bed.
851

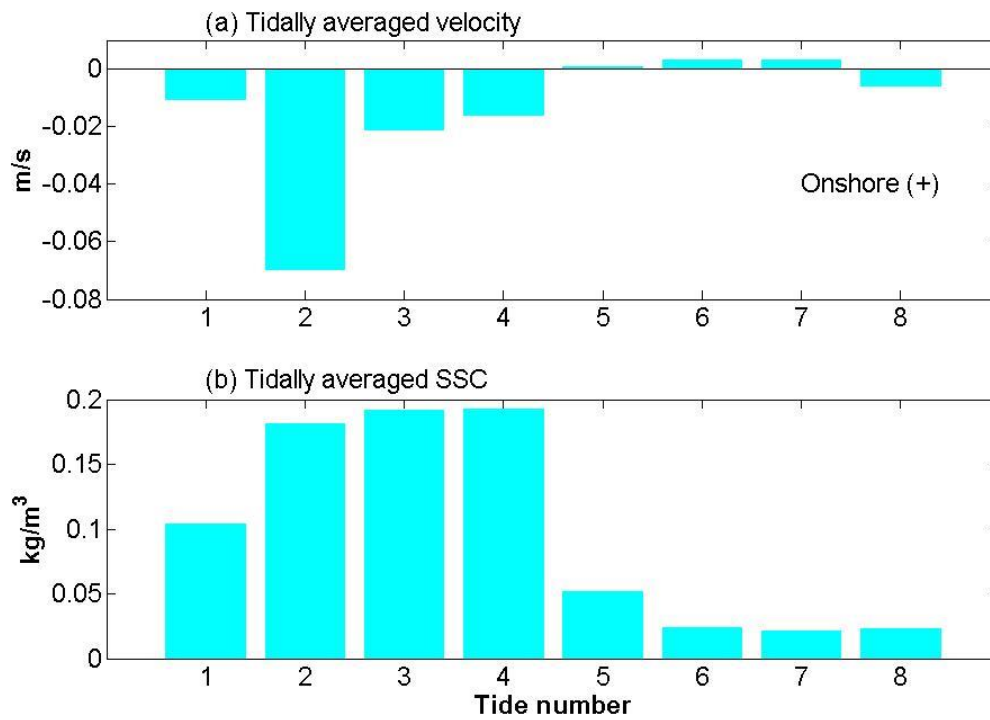


852
853 Figure 8: Bar graph showing the sediment flux rates at four different time scales for tidal periods
854 1-8 (see Eqs. 1-7). From left to right for a particular tidal period, the sediment flux rates

Fig

855 depicted are at the residual (tidally averaged), tidally varying, seiching, and wave frequencies.
856 The upper graph shows the tidal periods during a meteorological event characterized by
857 sustained winds of up to 9 m/s, while the lower graph denotes tidal periods during the calmer
858 period (wind speeds of 0-5 m/s) that follows. The onshore direction of flux is positive.

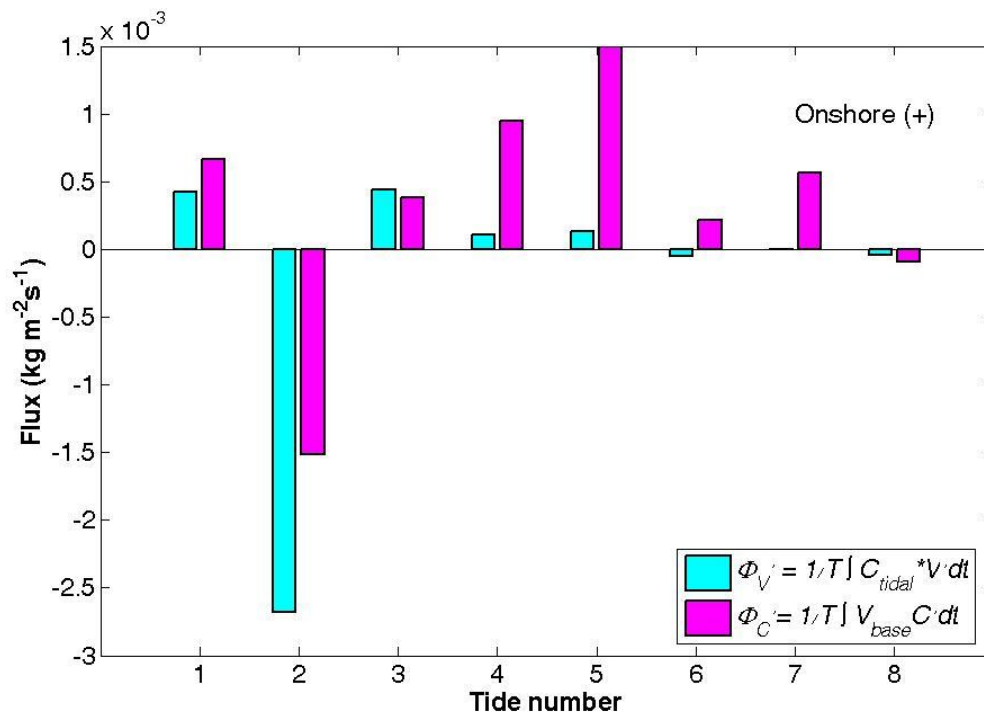
859



860
861
862
863
864
865

Figure 9: Residual, tidally averaged velocity (a) and suspended sediment concentration (b) over the 8 tidal periods of the experiment. Tides 1-4 occur during a meteorological event characterized by rainfall and sustained winds of up to 9 m/s. The remaining tides (5-8) occur during a calmer, dry period with winds of 0-5 m/s.

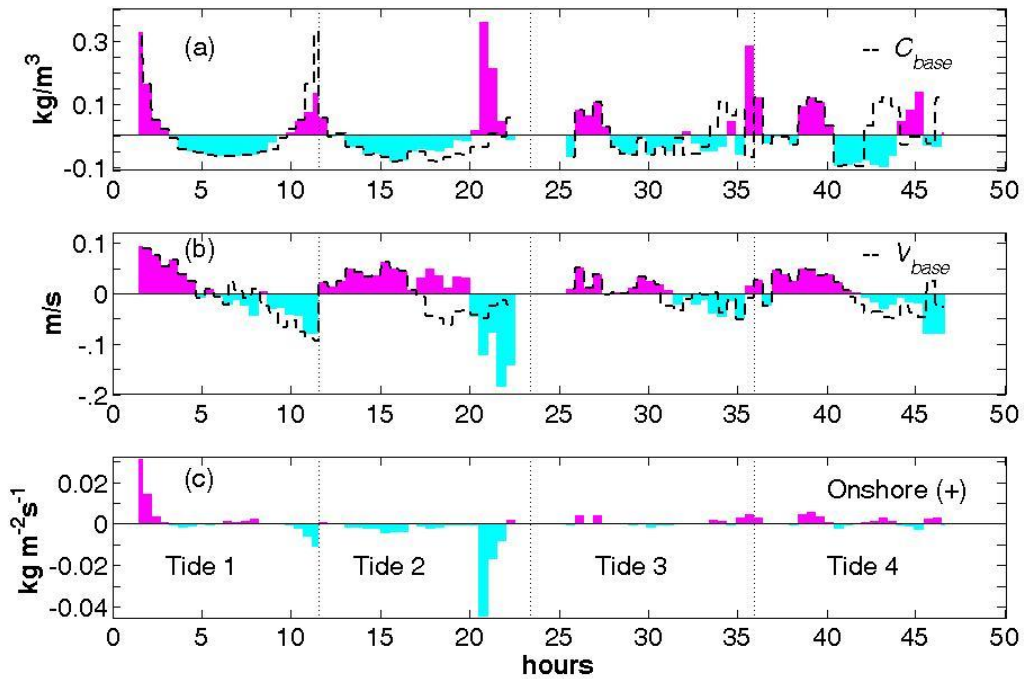
866



867
868
869
870
871
872
873

Figure 10: Comparison of tidally integrated sediment flux caused by asymmetries over a tidal cycle in tidally varying velocity ($\Phi_{V'}$) and SSC Φ_C , as defined in Eq. Tidal periods 1-4 coincided with a meteorological event with sustained wind speeds of up to 9 m/s, while tides 5-8 occurred in the calmer period that followed (winds of 0-5 m/s).

874



875

876

877

878

879

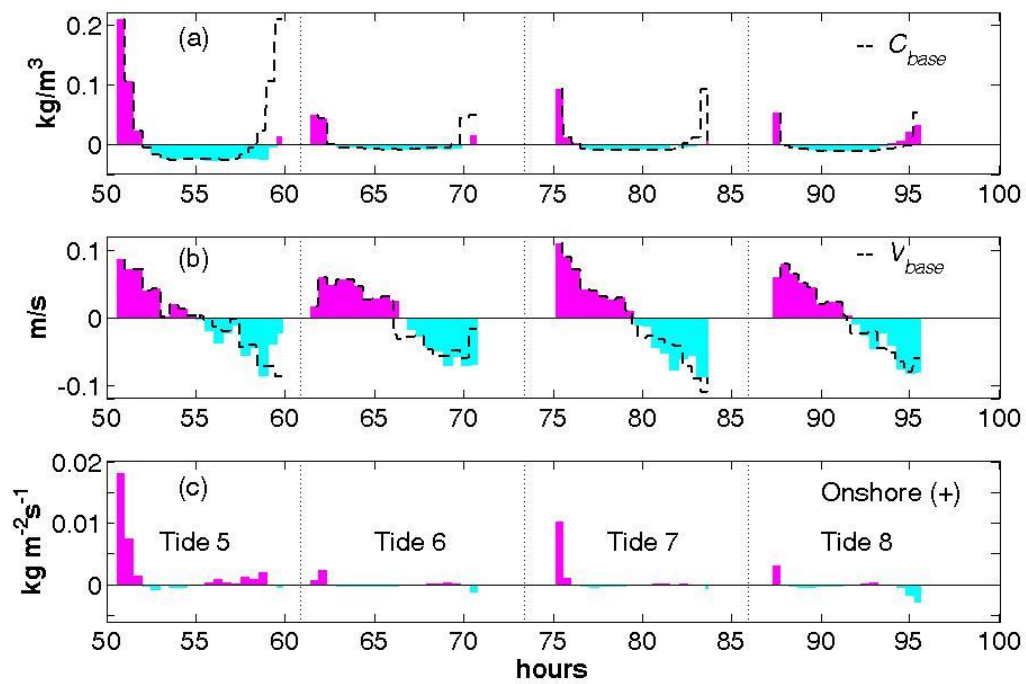
880

881

882

883

Figure 11: Tidal component of (a) suspended sediment concentration, (b) velocity, and (c) suspended sediment flux for tides 1-4, constructed using the 30 minute average (Eq. 5). Sediment concentrations and velocities are deviations from the tidal average. SSC and velocity components larger than the tidal mean are dark colored, while components less than the tidal mean are shaded light. Around $T/2$ for each tidal period, an even symmetrical function, C_{base} , has been constructed for SSC (dashed line in (a) and an odd function, V_{base} , has been constructed for velocity (dashed line in (b)). The vertical dotted line delineates tidal boundaries.

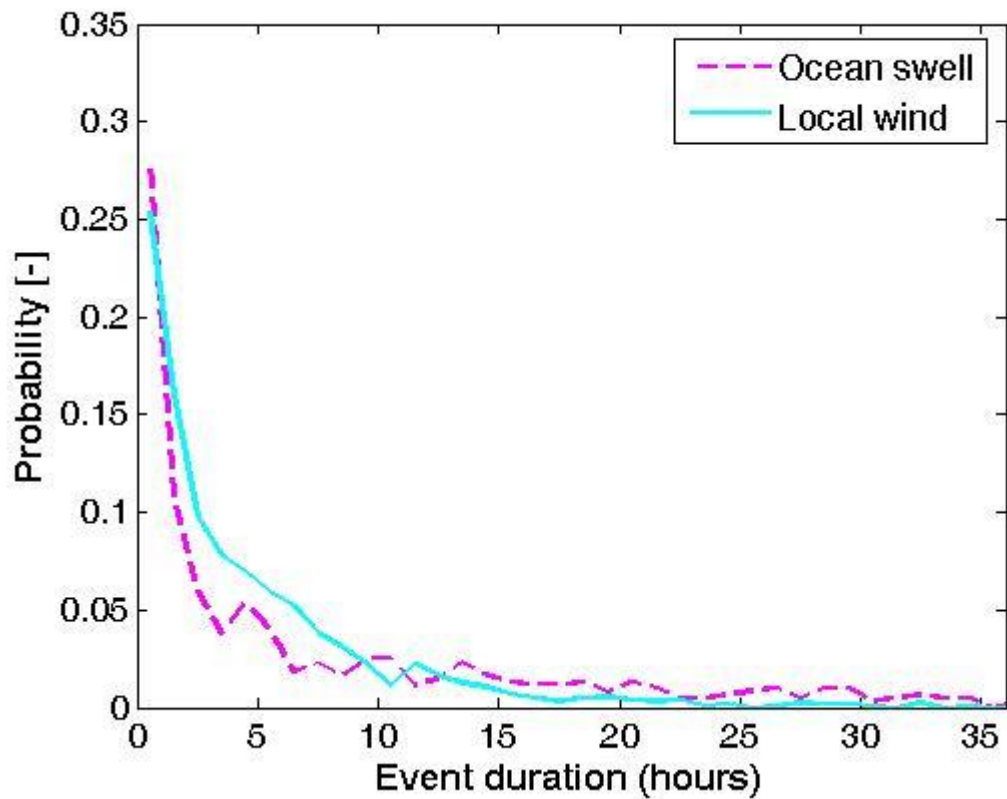


884
885
886

Figure 12: Tidal component of (a) suspended sediment concentration, (b) velocity, and (c) suspended sediment flux for tides 5-8, following the same format as Fig. 11.

Fig

887



888

889

890

891

892

893

894

895

896

897

898

Figure 13: Probability distribution of event length for offshore waves and local wind defined from 6 years of data (1999-2005). An event is defined as an offshore wave height exceeding 2.78 m and a wind speed exceeding 5 m/s, which represents any measurement greater than a standard deviation from the mean. The number of consecutive measurements that exceed the event threshold determines the time scale of the event. Over half (51%) of wind events occur over a time period of 3 hours or less, and over half (54%) of ocean swell events occur over a time period of 5 hours or less. Only 10 % of wind events, but 28% of offshore wave events, exceed 12 hours of duration.